Top Catal (2009) 52:1410–1424
DOI 10.1007/s11244-009-9321-2

ORIGINAL PAPER

# Applying Dynamic and Synchronous DRIFTS/EXAFS to the Structural Reactive Behaviour of Dilute (≤1 wt%) Supported $Rh/Al_2O_3$ Catalysts using Quick and Energy Dispersive EXAFS

**Mark A. Newton**

Published online: 24 June 2009


**Abstract** Examples of the application of a synchronous DRIFTS/EXAFS/mass spectrometry (MS) methodology to the study of dilute (≤ 1wt%) $Rh/Al_2O_3$ catalysts are discussed. These are used to explore the potential of this approach for understanding of the behaviour of supported metal catalysts "in a single shot", and in the often preferred regime of low (<1 wt%) loadings of active precious metals. Firstly, the sequential interaction of NO (323 K) and then CO (373 K) with reduced, 0.5 wt% $Rh/Al_2O_3$ catalysts is studied. Infrared spectroscopy indicates that two surface species (a bent $Rh(NO^-)$ and $Rh(CO)_2$ species) can be created using this sequential gas absorption/reaction method with minimal interference from other carbonyl or nitrosyl species. As such the potential for a reliable structural characterisation of the local structure of these species by EXAFS becomes possible. However, in contrast to the infrared spectroscopy, analysis of the EXAFS data also indicates that, even for such low loaded Rh systems, oxidative disruption of the Rh by the NO and CO is not complete and that bonding typical of small Rh clusters persists in both cases. The possible sources of this apparent spectroscopic difference of opinion are discussed. Secondly, 1wt% $Rh/Al_2O_3$ catalysts are studied using dispersive EXAFS at 573 K with 100 ms time resolution, during a redox switching event involving a reducing feedstock comprising just 3000 ppm of CO and 3000 ppm of NO. It is shown that highly useful and insightful time resolved and synchronously obtained XANES/EXAFS/IR data can be obtained even in this dilute Rh and more "realistic" case. Additional data, regarding the overall performance of the experiment, as currently implemented at the ESRF, along with a discussion of where enhanced performance might be yet still be gained, are also given.

**Keywords** Synchronous DRIFTS/EXAFS · Quick and energy dispersive EXAFS · Time resolved · CO NO reaction

M. A. Newton (✉)
The European Synchrotron Radiation Facility,
6 Rue Jules Horowitz, BP-220, Grenoble 38043, France
e-mail: newton@esrf.fr

## 1 Introduction

The increased benefits of studying catalytic systems of all denominations within multi-technique "operando" environments have become increasingly evident. [1] As long as the combinations of techniques utilised has been carefully thought through and executed such "one pot" investigations provide both a wealth of complementary and self consistent data.

Such approaches can massively improve the "duty cycle"of the investigative process—a consideration when using expensive and highly sought after resources such as synchrotron time—whilst at the same time minimising the possibility of problematic conflicts due to experiments carried out in separate systems, at differing times, and under inequivalent conditions.

Synchronously applied combinations of structurally direct X-ray based techniques, such as EXAFS, XRD, and SAXS/WAXS, together with vibrational spectroscopies (such as Raman [2–5] and infrared spectroscopies [6–12]), and techniques that give a global overview of catalytic performance (such as mass spectrometry and gas chromatography), are particularly attractive. A number of these types of experiments [2–12] have now been demonstrated, and it seems certain that they will become ever more powerful as the process of refining them, and developing

new ones, continues in response to the ever increasing desires of the catalysis, chemistry, and wider material science communities.

Here we consider one of these multitechnique approaches: a methodology that fuses transmission based X-ray probes with diffuse reflectance infrared spectroscopy and mass spectrometry. Originally developed at the University of Southampton, UK, [6–10] a resource of this type is now implemented on ID24 (dispersive EXAFS) a the ESRF, Grenoble [11, 12]. It is, however, a mobile experiment and can be utilised at other beamlines.

In this paper we focus on the sort information can we now achieve from the XAFS and IR components when considering "single shot" studies of essentially non reversible processes. It is these single shot type studies, on systems where facile repetition is not possible, that are in many ways, the most difficult for any experimental approach. This is especially the case when the concentrations of the components under study are low.

From this latter point of view a criticism that could be made, historically speaking, and particularly in the case of energy dispersive EXAFS, is that time resolved (in the seconds or below range) operando experiments, such as those considered here, have not been able to deal successfully with systems wherein active metal loadings are very low. In many cases, real catalytic application—for instance in hydrocarbon reforming, and three way catalysis for emission control—favours the utilisation of <1wt% levels of active metal.

A good case study in this respect is the time resolved study behaviour of Rh catalysts for understanding various aspects of the overall three ways process i.e. CO oxidation and NO reduction. Dispersive EXAFS applied (with, [6–10] and without [13, 14] synchronous infrared spectroscopy) has been very successfully applied to studying these issues, but generally only at the level of ca. 5 wt% loading of Rh [6–10, 13, 14] and at best (occasionally) at 2 wt% loading [10]. Even within this limited range of accessible Rh loadings, however, this approach has successfully pinpointed under what conditions and why particle size effects in, for instance, the interaction of NO with metallic Rh, appear and express themselves as they do [9, 10].

Nonetheless there are numerous drivers to try and make an experiment such as this as widely applicable and relevant as it can be. As such, here we show examples of its application to the study of the behaviour of $\leq$1 wt% Rh supported Rh catalysts derived from the implementation of this experiment for studies in two differing instances: firstly, for Quick scanning EXAFS measurements on a bending magnet EXAFS line (DUBBLE at the ESRF); and, secondly, at the undulator based dispersive EXAFS line of the ESRF, ID24. We use these examples to show what is currently possible and as the basis to try and suggest where one can improve capacity and what as yet untapped potential this experiment may still have.

## 2 Experimental

0.5 wt% Rh/$\gamma$-$Al_2O_3$ catalysts used in the Quick EXAFS studies were prepared as previously documented [6–10, 13, 14] via wet impregnation of $RhCl_3$ to $\gamma$-$Al_2O_3$ (Degussa Alon C). They were then dried overnight, and then sieved to a 110–80 μm fraction before being calcined in flowing 5% $O_2$/He for 6 h at 673 K. Prior to experimentation ca. 30 mg of sample was loaded into the experimental system (described in more detail below) at an effective bed density of <1 g $cm^{-3}$. This system permits temperature measurement (using a type K thermocouple inserted in to the sample bed) and control (Eurotherm) whilst permitting rapid switching of the feedstock the sample experiences using fast, gas (He) actuated 4 port valves (Valco).

Transmission scanning EXAFS experiments at the Rh K edge were performed on the DUBBLE CRG beamline at the ESRF using a Si [111] monochromator and ion chambers for detection. Gas feeds were used at 75 mL $min^{-1}$ and comprised either, He, 5% $H_2$/He, 5% $O_2$/He, 5% NO/He, or 5% CO/He. Samples were heated (under 5% $H_2$/He) to 573 K and then transiently exposed (ca. 120 s) to flowing 5% $O_2$/He before returning the feed to 5% $H_2$/He. This procedure removes any adventiously adsorbed residues whilst ultimately leaving the Rh in a reduced state [14]. Thereafter the samples were cooled under 5% $H_2$/He and then flowing He (at T < 373 K). At 323 K the reduced Rh samples where then exposed to 100 s of 5% NO/He whilst at the same time collecting mass spectrometry data and infrared spectra (at ca. 3 Hz). The resulting sample was then heated to 373 K under He and then exposed to flowing 5% CO/He whilst again mass spectrometry and IR data were collected. In between these treatments, at 323 K under He, after exposure to 5% NO/He at 323 K, and then subsequently after exposure to 5% CO/He at 373 K, scanning EXAFS spectra were recorded in Quick scanning mode (60–180 seconds per scan).

A reference sample, comprising 2 wt% $[Rh(CO)_2Cl]_2$ supported upon Degussa Alon C was also prepared using a metallic organic chemical vapour deposition [15, 16]. A standard Rh K edge EXAFS spectrum from this sample was collected at BM 29 at the ESRF.

Dispersive EXAFS experiments were carried out at ID24 at the ESRF using a Si [311] polychromator in Bragg configuration and utilising a FReLoN detector [17]. A Rh foil, was used to calibrate the resulting spectra. Samples were loaded into the same experimental apparatus as used for the scanning experiments. As detailed in [18] two further experimental components/modifications were utilised.

A second 5 mm diameter pyrolytic BN ring containing a Rh-free $Al_2O_3$ reference was used to normalise the sample absorption signal. This reference is held outside of the sample environment but at the same focal position of the X-ray beam as the sample itself. Secondly the vertical X-ray beam was defocused in the vertical direction to ca. 300 (from ca. 100 μm).

Gas flow rates were in this case 100 mL $min^{-1}$. In the energy dispersive experiments described below the 1 wt% $Rh/Al_2O_3$ sample—derived from wet impregnation of $Rh(NO_3)_3/HNO_3$ solution to $\gamma$-$Al_2O_3$ (Grace)—was heated to 673 K under 2% $H_2$/He and then cooled to 573 K before being subjected to a 10 s oxidative pulse of 2% $O_2$ in He. The dispersive EXAFS/DRIFTS experiment starts immediately after this with a switch to a reducing gas mixture (0.3% NO + 0.3% CO, balance He) for 300 s. This was followed by a switch back to the oxidising 2% $O_2$/He flow. Concurrent with the switch to the reducing feedstock collection of dispersive EXAFS spectra (78 ms per spectrum) and DRIFTS spectra (ca. 1.1 s per spectrum, single sided acquisition) was initiated. Single sided acquisition is the most basic mode of infrared data collection, wherein data is collected only during the forward movement of the spectrometer mirror. This results in a so called single sided interferogram and a lower signal to noise ratio than other forms of collection. As such, it is used here to provide an indication of a base level of performance in these sorts of experiments.

Throughout this process the mass spectrometer was used to monitor the gas phase composition in parallel to the two other spectroscopies.

Data reduction and EXAFS analysis was performed using PAXAS [19] and EXCURV [20] and where appropriate, using full curved wave multiple scattering.

## 3 Details and Some Quantification of the ESRF DRIFTS/EXAFS Experimental Set Up

The previous incarnation of this experiment, developed at the University of Southampton, UK, [6–10] utilised a cell based upon the minimal dead volume design concept of McDougall et al. [21]. This design therefore results in a very fast gas switching response. However, in order to achieve this the gas feedstock passes over, rather than through, the catalyst bed. As such the principal requirement of plug flow [22] is not met. Moreover, the maximal temperature realistically achievable in this system is ca. 673 K [8].

The experiment implemented at the ESRF [11, 12] takes a slightly different tack in that it exploits some of the intrinsic design features of a commercially available DRIFTS cell (Spectratech), wherein the gas flow does flow through, rather than simply over the sample. Moreover, this commercial cell does yield the possibility of achieving the much higher sample temperatures (ca. 1100 K[1]) that are of interest in a number of catalytically relevant situations. A schematic of how this cell arrangement is shown in Fig. 1.

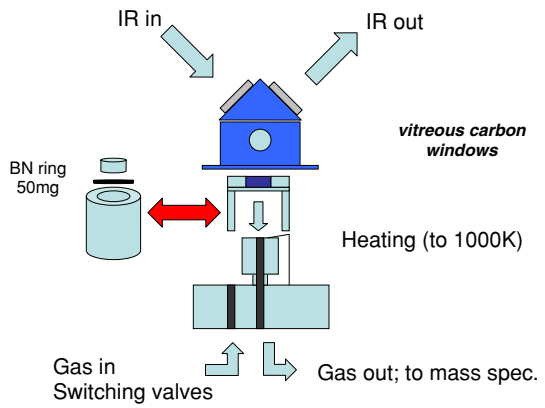


**Fig. 1** A schematic diagram of the experimental cell used at the ESRF for making synchronous DRIFTS/EXAFS/mass spectrometry measurements. Vitreous carbon windows are used to permit a high level of X-ray transmission through the cell whilst at the same time minimising potential interference to the XAFS measurement from glitches due to Bragg diffraction from more ordered windowing materials

The compromise one accepts in taking this route is that the canted IR windows inevitably lead to an increased dead volume as compare to the "flat top" design of McDougall (see for example, [21]). This, in turn, leads to a poorer overall response time of the system toward a change in atmospheric circumstances. Figure 2 shows responses obtained in this system for a switch from flowing He to a 5% CO/He flow as a function of the flow rate used and using 30 mg of calcined 0.5 wt% $Rh/Al_2O_3$ sample retained in a 5 mm diameter × 2.5 mm deep BN ring sample holder—yielding an effective bed density of 0.61 g $cm^{-3}$.

Two observations are worthy of note. Firstly is that from these data it can be implied that the dead volume of this cell is ca 2.5–3 mL. Second is that an unobstructed (minimal back pressure) flow of gas through the sample as presented can be achieved over a wide range of flows (up to 150 mL $min^{-1}$). However, this is only the case if the effective bed density is kept low. Over packing of the bed (even to 50 mg for the same bed volume) results in the rapid development of a backpressure in the system due to the resistance of the sample itself and a compromised switching response.

[1] Manufacturers specification for unmodified DRIFTS Cell. To date this system has been regularly and successfully used at 673 K [11, 12] and occasionally at higher temperatures (to 773 K). At the time or writing, however, extended and reliable use at temperatures significantly greater than 673 K has yet to be demonstrated for the system after modification for the combined X-ray/DRIFTS experiment.

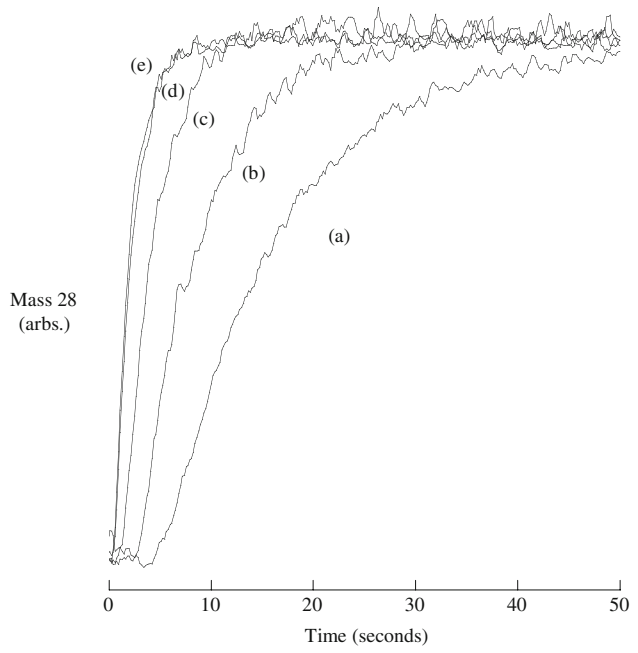


**Fig. 2** Temporal switching response of the system loaded with a pacified sample for switching from a flow of He to a flow of 5% CO/He as a function of flow rate: **a** 20 mLmin$^{-1}$; **b** 40 mLmin$^{-1}$; **c** 60 mLmin$^{-1}$; **d** 80 mLmin$^{-1}$; **e** 100 mLmin$^{-1}$

## 4 Results and Discussion

### 4.1 Low Temperature Sequential Reaction of NO and then CO Over Reduced 0.5 wt% $Rh/Al_2O_3$ Catalysts

Figure 3a and b show infrared spectra derived at specific points during and after the exposure of the reduced catalyst to firstly 5% NO/He (323 K), then He, and lastly (3b) to 5% CO/He at 373 K.

A number of species can be deduced to present at various times during these experiments on the basis of the DRIFTS [23—40], these being: $Rh^o(NO)$, bent $Rh(NO^-)$, $Rh(NO)_2$, $Rh(NO^+)$, $Rh(CO)(NO)$, $Rh(CO)_2$, and nitrate species. However, during these process the infrared yields no evidence of the consumption of –OH groups from the $Al_2O_3$ support (3300–3700 cm$^{-1}$).

What is clearly shown beyond this is that these species augment and sometimes attenuate with a variety of temporal characters and correlations. Figure 4a shows the temporal behaviour of a number of IR bands observed during the exposure of the sample to 5% NO/He; Fig. 4b does the same for bands appearing, attenuating, or appearing and then attenuating, during the subsequent exposure of the NO treated sample to CO at 373 K.

Taking the treatment of the reduced sample in NO at 323 K first. DRIFTS shows that nitrate species ($\nu$ = 1230, 1320 cm$^{-1}$)—that may or may not be associated with the

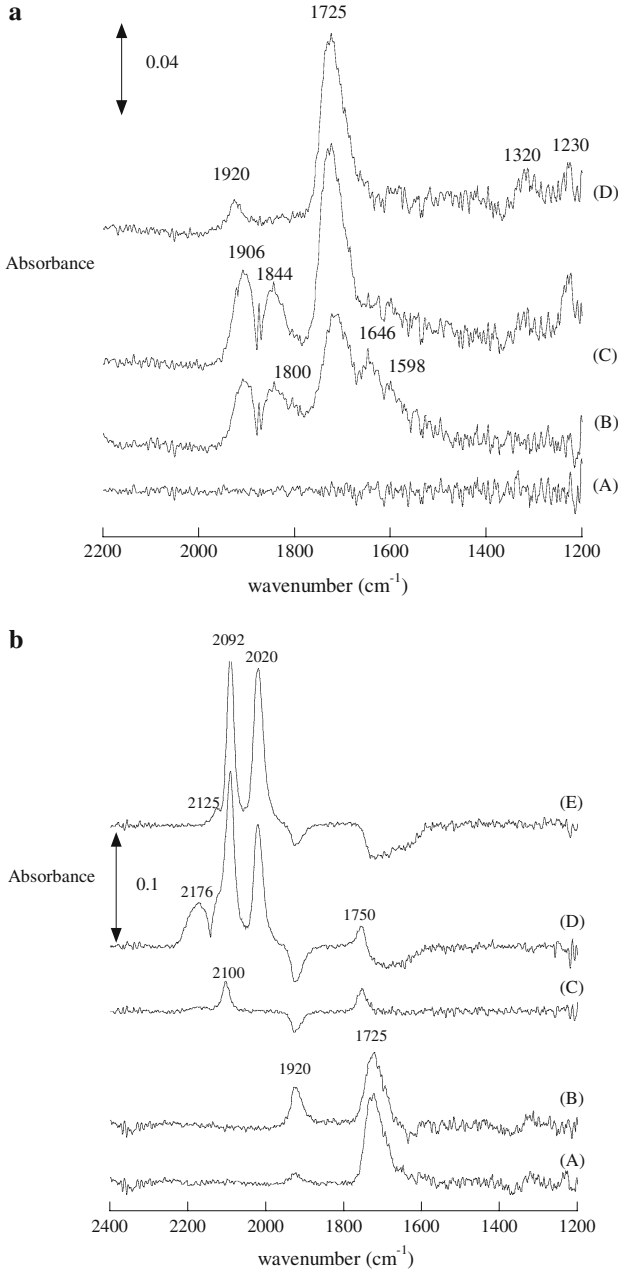


**Fig. 3** **a**. DRIFTS spectra taken during the exposure of a reduced 0.5 wt% $Rh/Al_2O_3$ sample to flowing 5% NO/He (from a He flow): (A) t = 0 s; (B) under NO at t = 8 s; (C) under NO at t = 60 s; (D) at 323 K, 100 s after switching flow back to He. Each spectrum is acquired in a single sided mode at ca. 3 Hz. **b**. DRIFTS spectra taken before and after switching the sample previously exposed to 5% NO/He at 323 K, to 5% CO/He at 373 K: (A) under He, post NO exposure at 323 K; (B) under He at 373 K; (C) at t = 1 s after the switch to 5% CO/He flow using spectrum (B) as a background; (D) after 60 s exposure to 5% CO/He; (E) at t = 200 s, 60 s after having switch the feed back to He. Again spectra were acquired in a single sided mode at ca. 3 Hz repetition rate. Spectra C to E utilise spectrum B as their background. As such the −ve bands observed at 1920 and 1700–1750 cm$^{-1}$ pertain to the consumption (during CO exposure) of the $Rh(NO^+)$ and $Rh(NO^-)$ species formed during the initial NO exposure

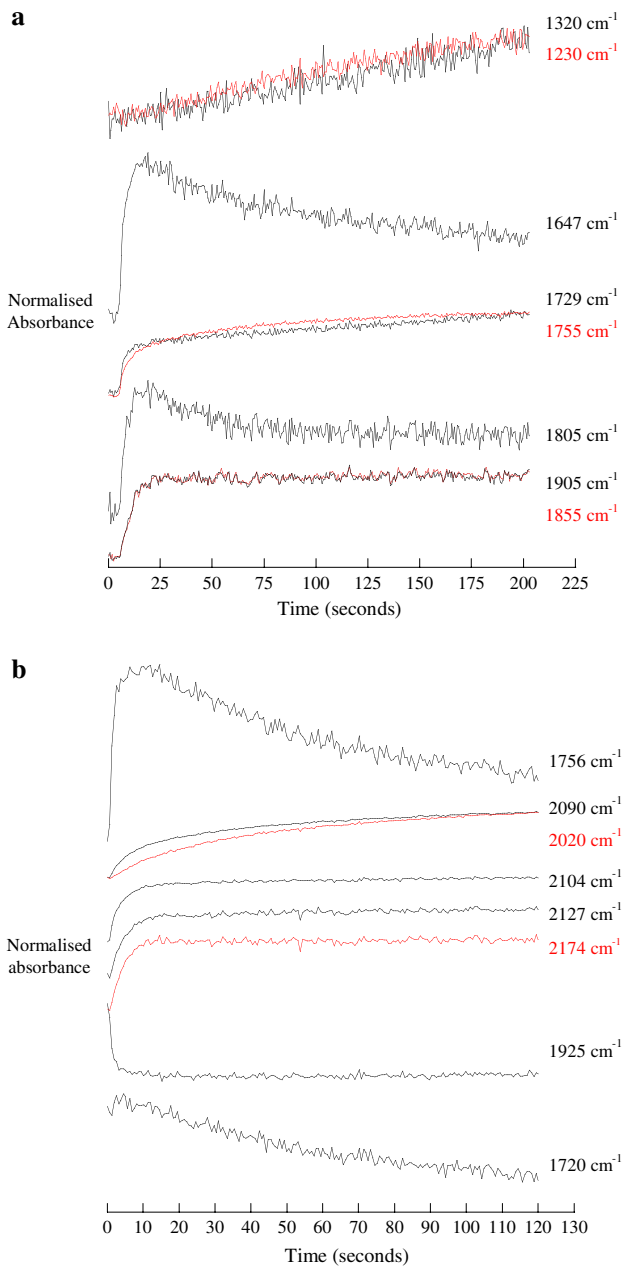


**Fig. 4** **a** The temporal dependence of a number of IR visible bands during exposure of the reduced 0.5 wt% $Rh/Al_2O_3$ sample to 5% NO/He. The band assignments are as follows: 1855, 1905 $cm^{-1}$, $NO_g$; 1925 $cm^{-1}$, $Rh(NO^+)$; 1805 $cm^{-1}$, asymmetric stretch of $Rh(NO)_2$; 1755 and 1725, overlapping components from symmetric stretch of $Rh(NO)_2$ and $Rh(NO^-)$; 1647 $cm^{-1}$, NO adsorbing on reduced "metallic" Rh centres; 1320 and 1230 $cm^{-1}$, $Al_2O_3$ or Rh nitrates. Each trace has been normalised to 1 at t = 200 s for comparison. **b** The temporal dependence of a number of IR visible bands during exposure of the 0.5 wt% $Rh/Al_2O_3$ sample, previously exposed to 5% NO/He at 323 K, to 5% CO/He at 373 K. The band assignments are as follows: 2174 $cm^{-1}$, $CO_{(g)}$; 1925 $cm^{-1}$; $Rh(NO^+)$; $Rh(NO^-)$, 1720 $cm^{-1}$; Rh(CO)(NO), 2104 and 1756 $cm^{-1}$; $Rh(CO)_2$, 2020 and 2090 $cm^{-1}$; 2127 $cm^{-1}$, CO adsorbed at a partially oxidised Rh site; and 1720, overlapping components from symmetric stretch of $Rh(NO)_2$ and $Rh(NO^-)$. Again, aach trace has been normalised to 1 at t = 200 s for comparison

Rh [28] are formed under 5% NO/He in apparently zero order fashion, in contrast to other Rh specific adsorbates. Even when relatively close together in the IR spectrum spectral features are found to behave in tangibly different ways (vis à vis the temporal intensity behaviour observed at 1729 and 1755 $cm^{-1}$). This differential behaviour (within a spectral range of ca. 30 $cm^{-1}$) appears to be linked to the behaviour of other spectral features (at, for instance, 1647 and 1805 $cm^{-1}$) that rapidly appear and then are more slowly removed.

The following reactions that unambiguously involve the Rh component during NO adsorption to a reduced 0.5 wt% system are thus implied to be

$$Rh^0 + NO_{(g)} \rightarrow Rh^0(NO)^{1647} \rightarrow Rh(NO^-)^{1725} \quad (1)$$

$$Rh + 2NO(g) \rightarrow Rh(NO)_2^{1800,1750} \quad (2)$$

$$Rh(NO)_2 \rightarrow NO_{(g)} + Rh(NO^+)^{1920} \quad (3)$$

The overall behaviour observed during NO exposure is broadly consistent with that observed previously using dispersive EXAFS/DRIFTS for 2 wt% $Rh/Al_2O_3$ [10] and with previous, static measurements [23–28]. However, in the current case, the species observed at ca. 1720–1750 $cm^{-1}$ dominate the DRIFTS spectra relative to, for instance $Rh(NO)^+$ (1920 $cm^{-1}$), to a far greater degree than in the 2 wt% Rh case [10]. Moreover, whereas the dispersive EXAFS/DRIFTS experiment on a 2 wt% sample pointed to the $Rh(NO)_2$ species being the end product after ca. 50 s NO exposure, these experiments show that at 323 K over a 0.5 wt% Rh sample it is the $Rh(NO^-)$ species (1720–1750 $cm^{-1}$) that is by far the majority, infrared visible end product of the NO exposure, with $Rh(NO)_2$ being a transient species formed within the course of the reactive events at 323 K. Indeed, the "majority" nature of the $NO^-$ is further reinforced when one considers that the $NO^+$ species should intuitively speaking have significantly larger extinction coefficient—on molecular dipole grounds—and as such appear much more strongly in the IR spectrum on a "molecule by molecule" basis.

In heating the sample from 323 to 373 K prior to CO exposure, we further observe that the relative amounts of $Rh(NO^+)$ increases at the expense of intensity associable with the $Rh(NO^-)$ species. This occurs in the absence of NO and with no visible indication of the involvement of the $Rh(NO)_2$ species. As such this would suggest a further, possibly kinetically limited, structural rearrangement of the surface bound Rh nitrosyls; one that implies a rehydbridisation of the NO species from a bent (sp2, 1 electron donor), to a linear (sp, 3 electron donor) and that is not a combination of reactions 1 and 3 [24] i.e.

$$Rh(NO^-)^{1725} \rightarrow Rh(NO^+)^{1920} \quad (4)$$

At the present level of analysis we cannot, however, say conclusively whether the majority of the Rh($NO^-$) species forms under 5% NO/He via a transient $Rh(NO)_2$ species (reactions 2 and 3 in sequence) or through a transient molecular NO species forming on "Rh metal like" entities (reaction 1), or indeed whether both possibilities contribute in parallel.

Exposure of the majority Rh($NO^-$) and minority Rh($NO^+$) species to CO at 373 K leads to the extremely "clean", formation of a $Rh^I(CO)_2$ species: a position consistent with the majority of the existing infrared based literature for CO exposure to reduced Rh systems of this loading on $Al_2O_3$ [29–37]. The only other species observed to remain after CO exposure is a CO feature at 2127 $cm^{-1}$. We associate this band with a minority linear CO species adsorbed at an partially oxidised Rh site [29].

From a transient perspective, however, there are again a number of interesting behavioural traits to be noted from the infrared component of the experiment. We can observe that the symmetric stretch of the $Rh^I(CO)_2$ species (2092 $cm^{-1}$) appears to grow at a faster rate than the asymmetric (2022 $cm^{-1}$). Part of this affect could be due to interference in this region from bands due to gas phase CO.

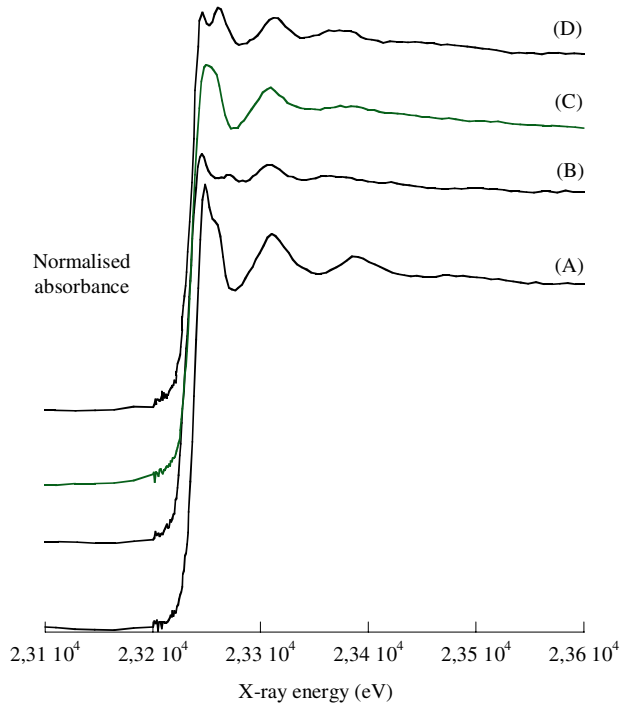


**Fig. 5** Normalised Rh K edge EXAFS derived from 0.5 wt% Rh/$Al_2O_3$: **a** "as prepared" (post calcination, prior to reduction), at RT (averaged over 7 × 3 min QuEXAFS scans); **b** under flowing 5% $H_2$/He at 573 K (averaged over 10 × 3 min QuEXAFS scans); **c** after exposure to 5% NO/He at 323 K (averaged over 10 × 3 min QuEXAFS scans); **d** after exposure of **c** to 5% CO/He at 373 K (averaged over 10 × 3 min QuEXAFS scans). The edge jump prior to normalisation was 0.1

However, we can also see that (initially) a further species is contributing to this difference. The bands observed in spectrum (C) of Fig. 3b identify the very rapid formation of a Rh(CO)(NO) species (2105 and 1755 $cm^{-1}$). This forms via the interaction of the CO with the $Rh(NO)^+$ (1920 $cm^{-1}$) species which is then removed from the surface in favour of the $Rh^I(CO)_2$ species. The majority formation of the $Rh^I(CO)_2$ species, however, appears to proceed (at a more leisurely pace) via direct reaction with the majority Rh($NO^-$) species.

Importantly, after the exposure to NO at 323 K, and subsequent reaction with CO at 373 K, essentially "clean" infrared signals, indicative the overwhelming predominance of either a Rh($NO^-$) species or a $Rh^I(CO)_2$ species, are observed. As such we might try to use EXAFS to determine the local structures and coordination of these species.

Figure 5 shows Rh K edge EXAFS data obtained for 0.5 wt% Rh/$Al_2O_3$ catalysts in normalised absorption form: (A) fresh sample under flowing He; (B) under 5% $H_2$/He at 573 K; (C) after exposure to 5% NO/He at 323 K; and (D) after subsequent reaction with 5% CO/He at 373 K.

Figure 6 shows the $k^3$ weighted EXAFS and associated theoretical fits for the first two cases: these being the fresh sample (under He at RT) and the reduced sample at 573 K under a 5% $H_2$/He flow. Table 1 summarises the local co-ordination and statistical data derived from the analysis.

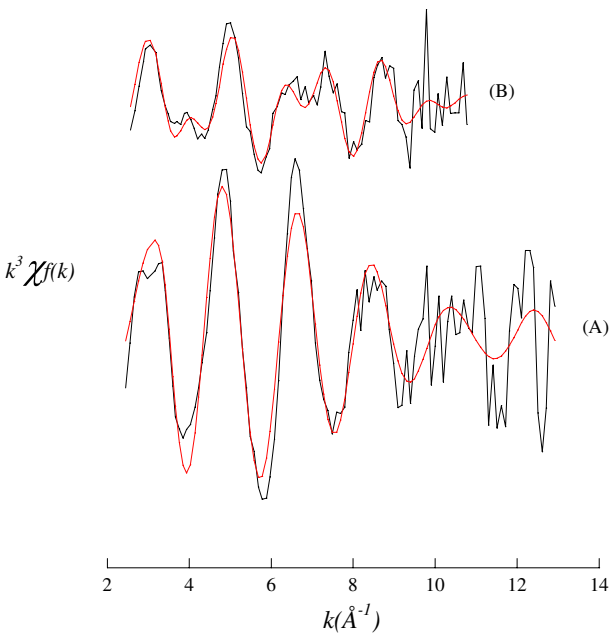


**Fig. 6** $k^3$ weighted EXAFS and fits derived from analysis in EXCURV for: **a** "as prepared" at RT (averaged over 7 × 3 min QuEXAFS scans); **b** under flowing 5% $H_2$/He at 573 K, (averaged over 10 × 3 min QuEXAFS scans). Structural and statistical data is given for both cases in Table 1

**Table 1** Summary of the structural and statistical parameters derived from analysis of Rh K edge QuEXAFS of the "as prepared" 0.5 wt% $Rh/Al_2O_3$ sample (measured at room temperature and under flowing He), and the same sample under forming 5% $H_2$/He at 573 K. Bracketed contributors show additional Rh shells that improve the fits but not to a degree that might reasonably be considered as statistically significant

| Sample | $k_{min}$ ($Å^{-1}$) | $k_{max}$ ($Å^{-1}$) | Scatterer | CN | R ($Å^{-1}$) | DW ($2\sigma^2$) | $E_F$ (eV) | R (%) |
|---|---|---|---|---|---|---|---|---|
| 0.5% $Rh/Al_2O_3$ "fresh" under He at RT | 2.5 | 13 | O | 3.4 | 2.038 | 0.008 | 2.316 | 43 |
| | | | Cl | 1.3 | 2.295 | 0.009 | | |
| | | | (Rh) | (0.6) | (2.712) | (0.005) | (0.9) | 40 |
| 0.5% $Rh/Al_2O_3$ at 573 K under 5% $H_2$/He | 2.5 | 12.5 | O | 1.8 | 2.01 | 0.017 | 3.6 | 53 |
| | | | O | 4.5 | 3.16 | 0.013 | | |
| | | | (Rh) | (0.6) | (2.59) | (0.02) | (3.3) | 50 |

The "as synthesised" sample shows an EXAFS response indicative of an oxidised ($Rh^{III}$) phase, though at this level of Rh dilution the precise structure of the oxide phase cannot be determined. Fitting of this data does, however, indicate a retention of a significant Cl co-ordination. The "reduced" form of the Rh produced in this instance is not amenable modeling as a typical *fcc* type entity. This EXAFS data can merely indicate that any "particulate" Rh that may be present is very small and intimately in contact with both oxygen from the support, and possibly oxygen that has not been removed by the thermal treatment of the starting nanosize $Rh_xO_yCl_z$ entities implied to have been derived from the initial calcination of the sample. Again, however, the precise nature of this form of the supported Rh, remains to be understood in any detail.

Figure 7 shows again shows $k^3$ weighted EXAFS data, in this case for the adduct formed at 323 K through exposure of the reduced system to 5% NO/He. Analyses of two structural models for this system are given and Table 2 shows the relevant structural and statistical data derived from the analysis in EXCURV.

Figure 8 and Table 3 depicts and summarise the structural information derived from applying three models of the Rh system that arises out of the subsequent exposure of the system (previously exposed to NO) to 5% CO/He at 373 K. In this case the results for three models of the majority $Rh^I(CO)_2/Al_2O_3$ system are given. Table 3 also details the structural and statistical information derived from the reference derived from MOCVD of $[Rh(CO)_2Cl]_2$ to the same $\gamma$-$Al_2O_3$.

In contrast to the fits shown in Fig. 2 (Table 1), in each of these cases a full multiple scattering approach was undertaken try to determine the structure of the $Rh(NO^-)$ and $Rh^I(CO)_2$ species derived from the reaction with NO.

The EXAFS data shows that both after exposure to NO at 323 K, and then again after exposure of the adduct thus generated to 5% CO/He, at 373 K, the predominant Rh species on the surface may be quite adequately modeled as square planar, surface organometallic species. Importantly,

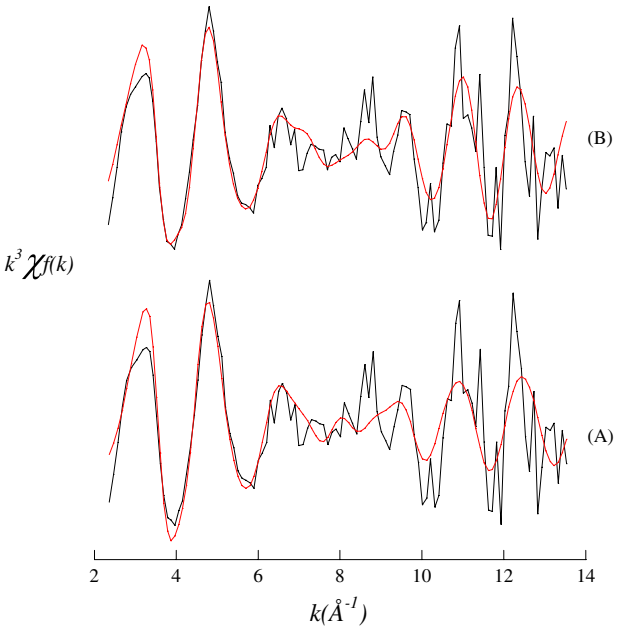


**Fig. 7** $k^3$ weighted EXAFS and fits derived from analysis in EXCURV for reduced 0.5% Rh $Al_2O_3$ after exposure to flowing 5% NO/He at 323 K and averaged over 10 × 3 min QuEXAFS scans. **a** shows a fit to the data using a square planar $(O_2)Rh(Cl)(NO)$ model and with an Rh–N–O bond angle of 120°. **b** shows a fit utilising the same square planar model but with a Rh atom added out of plane at ca. 2.67 Å from the central Rh atom. The R factor for the fit from 54% to 47.6% through the addition of this out of plane Rh co-ordination (see Table 2)

in both cases, Rh bonding to Cl atoms is clearly retained and completes the stable organometallic configurations. The net conversion between nitrosyl and carbonyl therefore proceeds through changes in Rh co-ordination to the oxide according to the number of ligands (1 NO or 2CO) that are sequestered from the gas phase.

The majority nitrosyl species, in accordance with the observations made in DRIFTS is well modeled with a single, bent (Rh–N–O = 120°), Rh–N–O bond: indeed this species is very similar to that previously shown to be

**Table 2** Summary of the structural and statistical parameters derived from analysis of Rh K edge scanning EXAFS obtained after reaction of the reduced 0.5 wt% $Rh/Al_2O_3$ sample with 5% NO/He at 323 K and fitted with two models of the system. (A) a square planar $(O)_2Rh(Cl)(NO)$ species with the Rh–N–O bond bent to 120°. (B) As model (A) but with an additional out of plane Rh scatterer representing potential contributions from residual "metallic" Rh nanoparticles. For these analyses full multiple scattering analysis was applied

| Spectrum | Model | $k_{min}$ ($Å^{-1}$) | $k_{max}$ ($Å^{-1}$) | Scatterer | CN | R ($Å^{-1}$) | DW ($2\sigma^2$) | $E_F$ (eV) | R (%) |
|---|---|---|---|---|---|---|---|---|---|
| A | $Rh(O)_2(Cl)(NO)$ | 2.5 | 13.5 | $O_S$ | 1 | 1.917 | 0.008 | 3.9 | 54.0 |
| | | | | $O_S$ | 1 | 2.028 | 0.003 | | |
| | | | | N | 1 | 2.043 | 0.0011 | | |
| | | | | Cl | 1 | 2.372 | 0.008 | | |
| | | | | $O_{(NO)}$ | 1 | 2.81 | 0.008 | | |
| B | $Rh^0 + Rh(O)_2(Cl)(NO)$ | 2.5 | 13.5 | $O_S$ | 1 | 1.946 | 0.007 | 4.415 | 47.64 |
| | | | | $O_S$ | 1 | 2.020 | 0.008 | | |
| | | | | N | 1 | 2.080 | 0.008 | | |
| | | | | Cl | 1 | 2.4 | 0.009 | | |
| | | | | $O_{(NO)}$ | 1 | 3.055 | 0.014 | | |
| | | | | Rh | 1 | 2.675 | 0.002 | | |

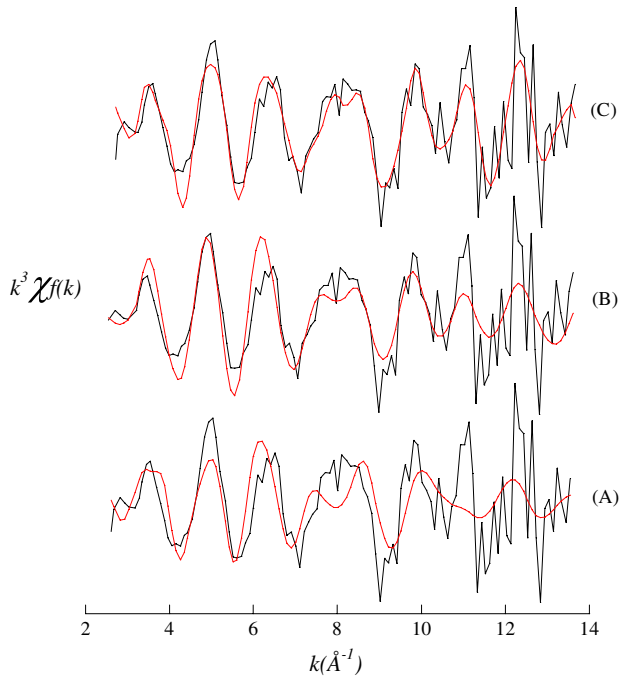


**Fig. 8** $k^3$ weighted EXAFS, and fits derived from analysis in EXCURV, for reduced 0.5% $Rh/Al_2O_3$ exposed to 5% CO/He at 373 K, after prior exposure to flowing 5% NO/He at 323 K. Again the data is an average over 10 × 3 min QuEXAFS scans. In this case three models to the data have been tested: **a** shows a "Cl-free" fit to the data using a square planar $(O_2)Rh(CO)_2$ model; **b** a square planar $(O)(Cl)Rh(CO)_2$ model; **c** shows the increased fit quality achieved by taking model (**b**) and again adding an out of plane Rh scatterer at ca. 2.67 Å to represent any residual bonding typical of metallic Rh. The analytical R factors fall from **a** 80% to **b** 66.6% to **c** 57.2% (see Table 3)

produced from the interaction of NO with adsorbed $Rh(CO)_2Cl$ species supported upon $Al_2O_3$ via MOCVD of $[Rh(CO)_2Cl]_2$ [15, 16].

Similarly the majority $Rh(CO)_2Cl$ species produced from the reaction of the $NO^-$ species with CO is, to all intents, identical to that formed via MOCVD of $[Rh(CO)_2Cl]_2$ to $Al_2O_3$ [15, 16] and indeed to majority geminal dicarbonyl species on the stoichiometric (1 × 1) $TiO_2$[110] surface [38] via MOCVD of the same organometallic precursor.

Nevertheless, the EXAFS yields evidence in both cases that the oxidative disruption of the starting Rh particles is not complete; it is necessary to add to the models of the species produced by these interactions Rh–Rh contributions at ca. 2.67–68Å in order to fit the EXAFS data (especially at high k). That this is the case is well reflected by the considerable improvement to the fits, both by eye and in the change in the R factor, that arise from the addition of a Rh–Rh component. By contrast, as already stated, and especially after the reaction with CO, the infrared component of the experiment yields no evidence for species forming that are indicative of the presence of Rh in any other form than the geminal species—for instance well known linear and bridging carbonyl species [29–36] that one would associate with the presence of metallic Rh particles.

### 4.2 Dispersive EXAFS of ca. 1 wt% $Rh/Al_2O_3$ Catalysts During a Redox Switch at 573 K Involving CO and NO

Figure 9 shows Rh K edge dispersive EXAFS data from a 1 wt% $Rh/Al_2O_3$ catalyst in (9a) raw absorption and (9b) $k^3$ weighted forms. These data were collected in 78 ms at 573 K at t = 0 s (spectrum (A), after brief oxidation of the Rh under 2 wt% $O_2$/He), and at the end of the exposure to

**Table 3** Summary of the structural and statistical parameters derived from analysis of Rh K edge scanning EXAFS from the 0.5 wt% Rh/$Al_2O_3$ sample previously reacted with 5% NO/He at 323 K and then with 5% CO/He at 373 K. Three models of the system have been investigated. (A) a square planar, Cl free, $(O)_2Rh(CO)_2$ species. (B) a square planar, $(O)(Cl)Rh^I(CO)_2$ species; (C) As model (B) but with an additional out of plane Rh scatterer representing potential contributions from residual "metallic" Rh nanoparticles. (D) results derived from the analysis of a pure geminal dicarbonyl system derived from MOCVD of $[Rh^I(CO)_2Cl]_2$ supported upon $\gamma$-$Al_2O_3$ [15, 16] to a 2 wt% loading. Again full multiple scattering was applied

| Spectrum | Model | $k_{min}$ (Å$^{-1}$) | $k_{max}$ (Å$^{-1}$) | Scatterer | CN | R (Å$^{-1}$) | DW ($2\sigma^2$) | $E_F$ (eV) | R (%) |
|---|---|---|---|---|---|---|---|---|---|
| A | $Rh(O)_2(CO)_2$ | 2.5 | 13.5 | $O_S$ | 1 | 2.065 | 0.013 | 7.3 | 79.89 |
| | | | | $O_S$ | 1 | 2.106 | 0.013 | | |
| | | | | C | 1 | 1.841 | 0.014 | | |
| | | | | C | 1 | 1.851 | 0.014 | | |
| | | | | O(co) | 1 | 2.993 | 0.014 | | |
| | | | | O(co) | 1 | 2.972 | 0.014 | | |
| B | $Rh(O)(Cl)(CO)_2$ | 2.5 | 13.5 | $O_S$ | 1 | 2.07 | 0.002 | 4.484 | 66.61 |
| | | | | Cl | 1 | 2.354 | 0.003 | | |
| | | | | C | 1 | 1.876 | 0.016 | | |
| | | | | C | 1 | 1.895 | 0.016 | | |
| | | | | $O_{(CO)}$ | 1 | 3.013 | 0.012 | | |
| | | | | $O_{(CO)}$ | 1 | 2.991 | 0.012 | | |
| C | $Rh(O)(Cl)(CO)_2 + Rh^0$ | 2.5 | 13.5 | $O_S$ | 1 | 2.035 | 0.004 | 5.9 | 57.20 |
| | | | | Cl | 1 | 2.314 | 0.003 | | |
| | | | | C | 1 | 1.922 | 0.016 | | |
| | | | | C | 1 | 1.840 | 0.016 | | |
| | | | | $O_{(CO)}$ | 1 | 2.956 | 0.015 | | |
| | | | | $O_{(CO)}$ | 1 | 2.819 | 0.015 | | |
| | | | | Rh | 1 | 2.696 | 0.009 | | |
| D | $Rh(CO)_2Cl]_2/Al_2O_3$ MOCVD reference | 3 | 14 | $O_S$ | 1 | 2.105 | 0.013 | 2.945 | 24.79 |
| | | | | C | 1 | 1.837 | 0.005 | | |
| | | | | C | 1 | 1.855 | 0.005 | | |
| | | | | Cl | 1 | 2.351 | 0.005 | | |
| | | | | $O_{(CO)}$ | 1 | 2.981 | 0.006 | | |
| | | | | $O_{(CO)}$ | 1 | 2.97 | 0.006 | | |

the reducing (0.3% CO + 0.3% NO, balance He) feedstock, (spectrum (B) at t = 300 s).

Figure 10 shows representative DRIFTS spectra from this experiment, again collected in a single sided mode of acquisition at ca. 1 Hz. Figures 11 and 12 show parameters that may be extracted from the EXAFS (Fig. 11, variation in white line intensity and edge position) and the temporal variation in IR visible bands observed during the switching experiment (Fig. 12).

In this reactive environment the combination of highly time resolved Rh EXAFS/XANES measurement with infrared spectroscopy highlights several interesting features of the redox chemistry of 1 wt% $Rh/Al_2O_3$ in an environment that is both a good model, in a number aspects, of real car catalyst operation, and a far more demanding test of the experimental methodology, in terms of the much lower levels of species in the gas phase (3000 ppm) liable to create IR active adsorbates, and the increased temperature.

The data shown in Fig. 9 show that we are now able to obtain acceptable XANES data from a 1 wt% Rh sample, and with an edge jump of ca. 0.1, in less than 100 ms. This data is certainly good enough to start assessing changes in the Rh K edge XANES during processes such as these.

It is also clear from these spectra (Fig. 9b) that we are starting to be being able to obtain EXAFS data under more realistic conditions, and in a fraction of a second, even for these 1 wt% Rh catalysts. Clear EXAFS structure, indicative of the formation of initially oxidic, and latterly reduced nanoparticulate Rh, can be observed within the energy range collected, even for acquisition times of <100 ms.

From the XANES we see that in the reductive switch, though there is a very rapid decrease in the measured white

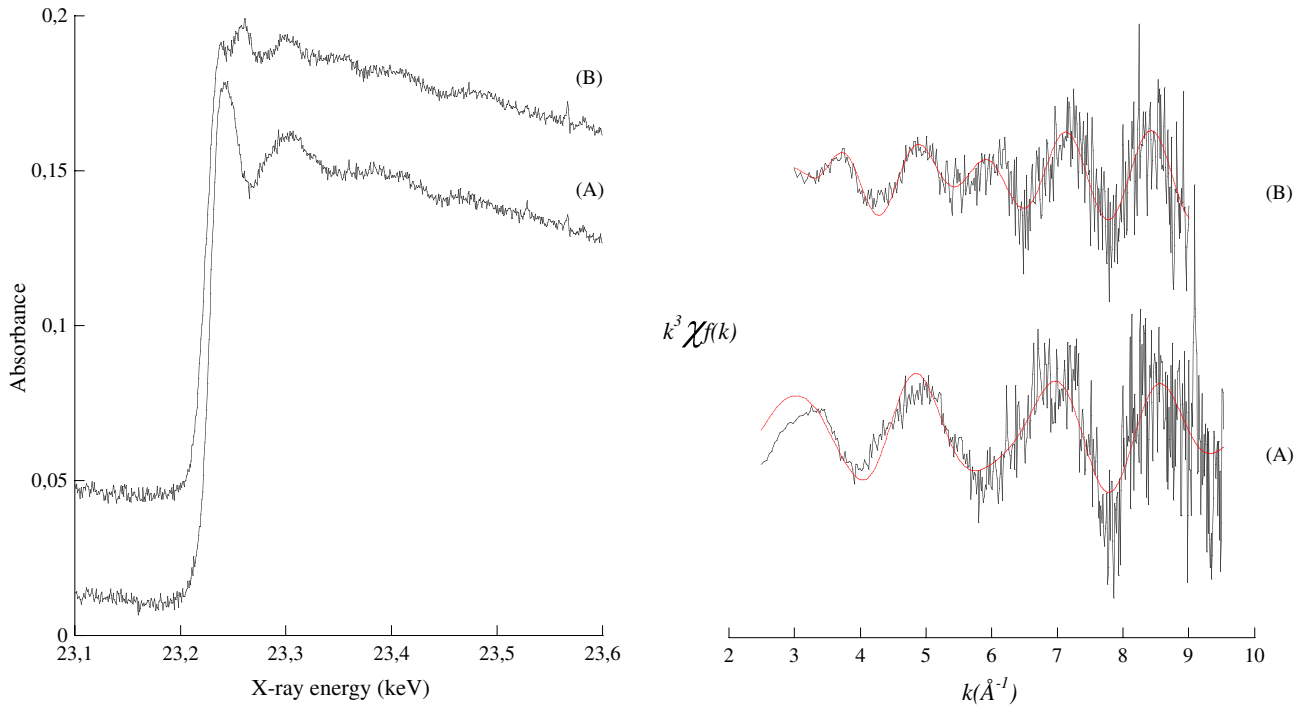


**Fig. 9** Rh K edge energy dispersive EXAFS data in raw absorbance form (*left* panel) and $k^3$ weighted form (*right*) derived from a ca. 1 wt% Rh/$Al_2O_3$ at 573 K and in oxidised (**a**) and reduced (**b**) states. Spectra collected in 78 ms

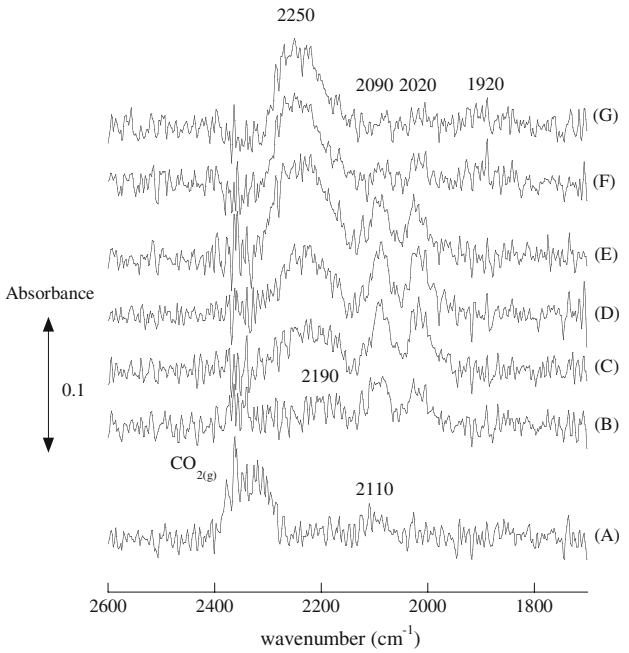


**Fig. 10** Single sided DRIFTS spectra taken in situ at 573 K, with a 1.2 s repetition rate resolution, during the exposure of a 1 wt% Rh/$Al_2O_3$ sample to firstly a reducing (0.3% CO + 0.3% NO, balance He) and secondly a net oxidising (2% $O_2$/He) reaction mixture. **a** first spectrum 1.2 s under net reducing atmosphere; **b** 10 s after reducing switch; **c** 60 s, **d** 100 s; **e** 250 s; **f** 275 s—25 s after switch to net oxidising conditions; **g** 350 s (100 safter switch to oxidising conditions)

line intensity, the measured Rh K edge position shows a tangibly different temporal behaviour. From this we may divine that, in this case, it is no simple matter to understand the formation of the reduced phase solely on the basis of the XANES and simple notions regarding $Rh^{3+}$ or $Rh^0$ oxidation states. A number of effects may be contributing in the XANES in this case and potentially relate to changes in Rh nanoparticle size and/or the potential speciation of the Rh into species of oxidation state other than $Rh^{3+}$ or $Rh^0$.

Here the infrared very much comes into play showing firstly that the formation of the $Rh^I(CO)_2$ species correlates well with the observed changes in edge position during the first 70 s of reaction, wherein the bulk of the shift in Rh K edge energy is achieved (Fig. 11). Conversely there is IR evidence for a CO species that has a temporal character much more like that observed for the initial changes in white line intensity—a high wave number CO species appearing at around 2110 $cm^{-1}$. In fact the appearance of this species in the system is so rapid that it is visible in first second of the switch to a reducing environment—during which time the first IR spectrum is collected—and concomitant with the transient burst of $CO_2$. Further, it is also rapidly removed from the surface, again in tandem with a rapid burst of $CO_2$ production when a switch is made to the oxidising feed. The absence of the simultaneous appearance of a second band that should be observable ca. 1750 $cm^{-1}$ would mitigate against this being due to the formation of a Rh(CO)(NO)

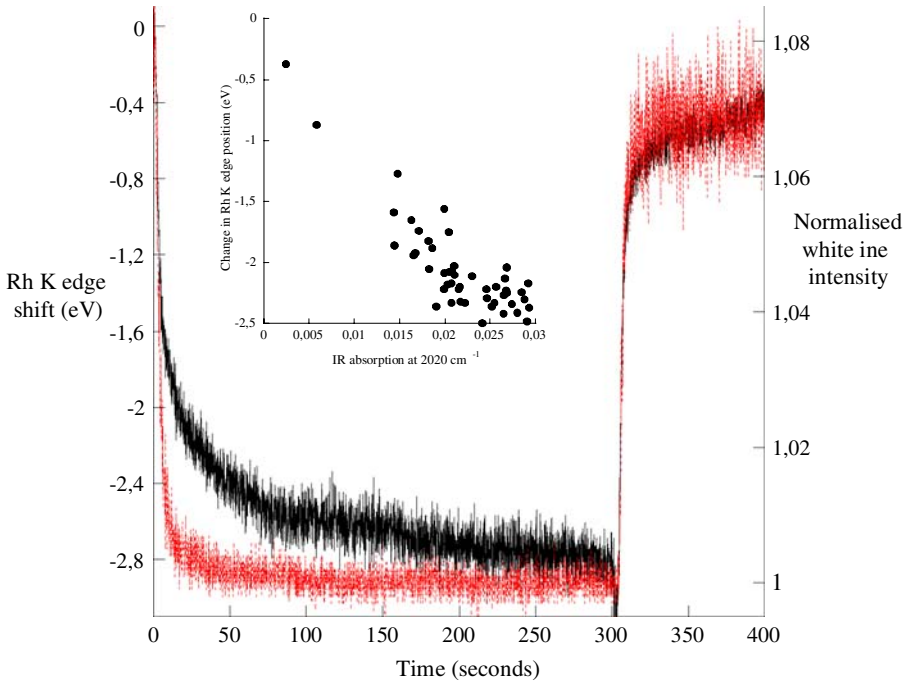


**Fig. 11** The temporal shift in Rh K Edge position (*black*), and *white line* maximum intensity (*red*) during redox switching over ca. 1 wt% $Rh/Al_2O_3$ at 573 K. The inset shows the extracted correlation between the shift in Rh K edge position with the appearance of the $Rh(CO)_2$ species (see also Fig. 12) for the first 70 s after switch to a reducing (300 ppm CO + 300 ppm NO) feed

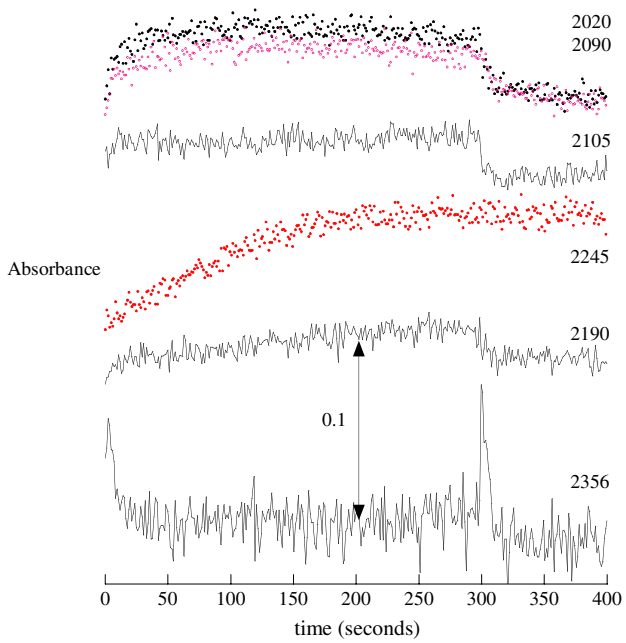


**Fig. 12** The temporal dependence of a number of IR visible bands during a redox switching experiment over a 1 wt% $Rh/Al_2O_3$ sample at 573 K; The band assignments are as follows: 2356 $cm^-$ $CO_{2(g)}$; 2020 and 2090 $cm^{-1}$, $Rh(CO)_2$; 2105 $cm^{-1}$, CO adsorbed at a partly oxidised Rh site; 2245 $cm^{-1}$ NCO species adsorbed upon $Al_2O_3$; 2190 $cm^{-1}$ Rh(NCO) species

species (as was observed in the previous example). Instead, we might associate the removal of the initially oxidised Rh, as observed in the XANES, together with $CO_2$ formation, with this 2110 $cm^{-1}$. This is consistent with previous concentration modulation experiments using DRIFTS spectroscopy [39] where the same IR observable CO species was directly associated with CO oxidation by $O_2$ at 573 K and over a 2 wt% $Rh/Al_2O_3$ catalysts.

Similarly the slower accumulation of $Rh(CO)_2$ species, that correlates with the change in the position of the Rh K edge jump during the first 70 s after the redox switch, indicates that under these conditions CO can effectively sequester Rh into what is, at 573 K, a relatively inactive species. It would appear that this may the principal reason for the differential response between the white line measurements and the edge position for $T < 70$ s after the initial gas switching event: we may well be forming $Rh^0$ clusters but we are also forming substantial levels of isolated $Rh^I$ species that are stable enough at 573 K to be observed. This, at least from an EXAFS point of view is consistent with previous dispersive EXAFS investigation of CO oxidation over Rh catalysts over 5 wt% $Rh/Al_2O_3$ samples [13].

A further band showing slow, zero order growth during the reducing cycle is observed at 2190 $cm^{-1}$. This band is associable with the formation of Rh(NCO) [40–42] species and rapidly disappears after the switch back to oxidising conditions, in tandem with the other carbonyls species, and concomitant with a burst of $CO_2$ production.

NCO species adsorbed on the $Al_2O_3$ (around 2245 $cm^{-1}$, [10, 43]) also accumulate in an essentially linear manner with time. However, unlike the Rh(NCO) species at 2190 $cm^{-1}$, they do not disappear from the

surface when the feed is switched from reducing to oxidising. Under these "dry" (no vapour phase $H_2O$) circumstances, therefore, they represent a "dead end" in terms of any catalytic utility.

Finally a pair of IR bands at 1650/1566 $cm^{-1}$, most likely indicative of the formation of carbonates also form slowly during the reductive switch and, for the most part, appear to be stable under the subsequently applied oxidising conditions.

## 5 Discussion, Summary, and Outlook

The experiments delineated here clearly show that the combined DRIFTS/EXAFS experiment currently implemented a the ESRF can provide a powerful experimental platform to start to address the structural-reactive behaviour of dilute metal catalysts under progressively more realistic conditions. Both quick scanning and energy dispersive EXAFS variant may be applied equally within the same sample environment, and in transmission mode; the experimental design does not (yet) permit fluorescence yield measurements.

It has been shown that one can utilise scanning EXAFS in transmission, before and after experimentation, yet still retain a highly useful time resolved component to the experiment using the DRIFTS. The study made here indicates that even for very small reduced Rh particles neither NO, or subsequently CO appears able to completely disperse Rh into isolated organometallic centres; some evidence for the persistence of Rh–Rh bonding is always found in the systems we have measured.

Conversely for these catalysts, and for the treatments given, IR indicates that we can essentially isolate some of the organo-Rh species formed during these interactions.

As such, though the IR indicates that we might start to address their individual structures with some degree of confidence using EXAFS, the EXAFS itself clearly indicates that that the IR component of the experiment appears not to be telling the whole story and a genuine attainment of a mono-phasic structural situation appears not to have arisen even in these dilute cases.

What we can say with some confidence in this case, is that the Rh that is dispersed into isolated organometallic centres in the first (scanning EXAFS) example, after NO or CO exposure is always associated with Cl. The "bent" surface nitrosyl and geminal dicarbonyl species can quite adequately be described—though not definitively assigned—as square planar species that have either one or two surface linkages according to whether the ligand(s) sequestered from the gas phase is NO or CO, respectively. These structures are essentially identical to those derived from the direct absorption and reaction with NO of the organometallic $[Rh(CO)_2Cl]_2$ to $Al_2O_3$ previously described [15, 16].

At present we might postulate that the reason for the persistence of EXAFS visible Rh–Rh interactions might lie in the results of any dissociative adsorption of the NO [44, 45] or subsequently, CO [46–48]. The products of any low level dissociation would be invisible to the mid range infrared and yet could quite easily act to curtail oxidative redispersion by adsorbing in high symmetry sites [48]—effectively holding Rh atoms together and preventing their dispersion into monodisperse Rh nitrosyl or carbonyl species—or simply blocking the sites from whence oxidative disruption is promoted.

The formation of both low levels of both $Rh(NO^+)$ and then a carbonyl absorption band at 2127 $cm^{-1}$ could be regarded as circumstantial evidence that this may well be the case. Both of these species have been show to require [7, 8], or have been associated with [29], oxidised Rh sites. In the current case the most likely source of a low level of such sites is dissociation adsorption of a small fraction of the NO at 323 K or the CO at 373 K.

At this point we note that the QuEXAFS measurements reported here derived from experimentation on a bending magnet source. To obtain data where some form of quantitative EXAFS analysis may be undertaken, for these low loaded samples around 1800 s of acquisition time QuEXAFS scans was required in the current study. The absolute flux and brilliance that can be obtained using such a bending magnet source are relatively low (by factors of $>10^2$–$10^3$) in comparison with insertion device (wiggler/undulator) based lines at 3rd generation sources. In the absence of other factors therefore, one might conclude that similar quality (transmission) EXAFS data could be easily obtainable on such 3rd generation insertion device sources in the ca. 1.8–18 s given the application of a monochromator system that can provide the requisite forward–backward scanning rates and function under the increased heat loads that these insertion devices produce. Though this has been clearly demonstrated as possible [49], this sort of fast single shot scanning EXAFS measurement is hardly ever reported in the literature—and even then generally only for XANES [5, 49, 50]. As such the full potential of the scanning EXAFS experiment in this respect currently remains to be achieved within the paradigm of a user facility that is consistently available to the various communities that may benefit from it.

By the same token, however, it must surely be only a matter of time before this situation is resolved, as there is a clear and present need for this sort of capacity[2]: the

[2] Since the compilation and submission of this paper a fast (<<1 secs/scan) Quick scanning EXAFS resource of the sort identified as being sorely needed has indeed become available (at

application of dispersive EXAFS across the energetic bandwidth that is of interest to the catalysis and materials science communities is far from complete and beset with numerous issues that come as part of the dispersive setup itself, and particularly when applied to systems of this "heterogeneous" nature [18]. It is noteworthy that the demonstration of dispersive EXAFS for the study of heterogenous catalysts based upon, for example, first row transition metal components is, to all intents, absent from the literature.

From the point of view of energy dispersive EXAFS, the data reported here represent a further step forward in our ability to obtain useful data on such low loaded systems and to fully realising the great potential that this technique has to offer in this field: the catalysts studied here are 5 times more dilute in Rh than have been utilised in most previous studies, [6–10, 13, 14] and twice as dilute than the previous best measurements reporting any form of analyseable EXAFS. [10, 37] This results from two areas where recently we have increased our understanding of how to translate the X-ray bandwidth applied to the sample from an undulator based source, into useable EXAFS when the sample comprises materials that have an intrinsically less than perfect spatial homogeneity. The first is a heightened appreciation of exactly how important scattering from the sample itself is, and to what level it needs to be accounted for, in a dispersive experiment. The second is an increased appreciation of how big and how stable the X-ray beam needs to be to average over, and avoid significant "scanning" of, the intrinsic spatial non homogeneity of the samples. If such a "scanning" situation arises any chance of restoring EXAFS data from a given sample in a single shot experiment rapidly evaporates; in this sense these sorts of materials are an acid test of just how stable the applied X-ray beam is [18].

In contrast to the dispersive EXAFS component of the experiment, the limitations of the DRIFTS component are, to all intent and purposes, those of any DRIFTS experiment, as the experimental geometry is not disturbed by the combination with X-ray measurements made in transmission. In this respect the example given here for dispersive EXAFS/DRIFTS might be regarded as indicative of a "worst case" (or at least the "worst" studied thus far using this methodology). Useable IR based information has been obtained despite the very low levels (3000 ppm each) of CO and NO present, the low levels of Rh, the elevated temperatures, and the use of the most basic method of data collection allowed by the IR spectrometer.

Given that mirror/detector alignments, and sample presentation are as they should be, the DRIFTS component of this experiment is therefore currently prisoner to the flux/brilliance that can be derived from a conventional bench top IR spectrometer. Incremental improvements to the performance of this experiment from the IR perspective can be foreseen, but, until such time as a serious improvement in the flux/brilliance of the IR source itself department can be made then it would seem that what is published here, and what has been achieved previously, [6–11] may well represent reasonable estimates of what will be possible in a single shot from this experiment. One might further note that in all the studies made thus far using this methodology have utilised highly infrared friendly chromophores (such as CO and NO); what one might be able to achieve in systems where species that are far less IR active (for example, –OH, CH, NH, stretches and bending modes) has yet to be seen.

In these respects the possibility that one might utilise the IR radiation produced in the synchrotron—possibly taken from a bending magnet adjacent to the insertion device being used for the structural investigation—for these sorts of studies seems, at the moment, the only alternative to making this experiment more powerful. The utilisation of synchrotron infrared is far from new [51–55]. However, this possibility has generally been aimed either at microscopy or at the far infrared rather than the mid-range spectroscopy. That said, the non thermal nature of synchrotron IR [56] and its potential for much greater brilliance (by a factor of ca $10^4$) may well provide the means the way for achieving improved performance (even if the absolute flux is not massively different from a bench top instrument) for instance, in terms of intrinsic signal to noise, or the ability to deal with much smaller samples. The latter case will certainly be important when trying to study many catalytic systems of interest where relatively "soft" edges are combined with support materials that are relatively absorbing in nature, and available bed diameters dwindle to $\leq$1 mm. Even in the mid range infrared, therefore, it may be the case that using a synchrotron based infrared source may still provide a significant way forward for these types of measurements. For a recent example using an infrared microscopy approach see Ref. [57].

## 6 Conclusions

The in situ combination of time resolved X-ray measurements, such as EXAFS, with vibrational spectroscopies, such as infrared, is both seductive and potentially powerful methodology for the investigation of catalysts, catalytic

Footnote 2 continued
the Swiss Light Source) to a wider user community. The author is given to understand (and sincerely hopes) that other resources of this nature are planned elsewhere, and will pass into the realm of accessible user facilities in the relatively near future. Further information regarding this new type of QUEXAFS resource can be found in [58, 59] or (http://sls.web.psi.ch/view.php/beamlines/superxas/).

processes, and materials research in general. It has been shown that the unique and highly complementary time resolved structuro-reactive information that the dispersive EXAFS/DRIFTS methodology provides can be applied under progressively more realistic "environmental" circumstances, and, for instance, at $\leq$1 wt% loading of the metal of interest.

**Acknowledgments** The ESRF is thanked for access to facilities and for the funding to develop this experiment and the offline facilities wherein it is housed. Florian Perrin, Trevor Mairs, Pascal Dideron, Gemma Guilera, Olivier Mathon, Sakura Pascarelli and Anna Kroner at ID24 are thanked for their support and the various contributions they have made to the development of the experiment. Anna Kroner is especially thanked for the synthesis and EXAFS spectrum of the supported $Rh(CO)_2Cl/Al_2O_3$ reference sample. Wim Bras and Sergei Nikitenko at DUBBLE are acknowledged for the provision of the beamtime and the support given during the experiment. Andy Beale and Fouad Soulimani (University of Utrecht) are also thanked for sharing of the DUBBLE beamtime used to collect the scanning EXAFS/infrared data reported here. The author is extremely grateful to Masahide Miura, Toyota Motor Corporation, Naoyuki Hara, Toyota Motor Europe, and Yasutaka Nagai, Toyota Central Research and Development Laboratories, for their longstanding commitment to research and development at ID24 and for the permission to use the Energy dispersive/DRIFTS data shown in this paper. Lastly the author would like to thank Augusto Marcelli, INFN-Laboratori Nazionali di Frascati, Italy, for discussions and information regarding new possibilities for exploitation of synchrotron based infra red light.

## References

1. Weckhuysen BM (2003) Phys Chem Chem Phys 5:4351–4360
2. Boccaleri F, Carniato F, Croce G et al (2007) J Appl Cryst 40: 684–693
3. Tinnemans SJ, Mesu JG, Kervinen K, Visser T, Nijhuis TA, Beale AM, Keller DE, van der Eerden AMJ, Weckhuysen BM (2006) Catal Today 113:3–15
4. Beale AM, van der Eerden AMJ, Kervinen K, Newton MA, Weckhuysen BM (2005) Chem Commun 301:5–3107
5. Briois V, Lutzenkirchen-Hecht D, Villain F, Fonda E, Belon S, Griesebock B, Frahm R, Phys J (2005) J Phys Chem A 109: 320–329
6. Newton MA, Jyoti B, Dent AJ, Fiddy SG, Evans J (2004) Chem Commun 21:2382
7. Newton MA, Dent AJ, Fiddy SG, Jyoti B, Evans J (2007) Catal Today 126:64–72
8. Newton MA, Dent AJ, Fiddy SG, Jyoti B, Evans J (2007) Phys Chem Chem Phys 9:246–249
9. Dent AJ, Evans J, Fiddy SG, Jyoti B, Newton MA, Tromp M (2007) Angew Chem 46:5356–5358
10. Newton MA, Dent AJ, Fiddy SG, Jyoti B, Evans J (2007) J Mater Sci 42:3288–3298
11. Newton MA, Belver C, Martínez-Arias A, Fernández-García M (2007) Nat Mater 6:528–532
12. Newton MA, Belver-Coldeira C, Martínez-Arias A, Fernández-García M (2007) Angew Chem Int Ed 46:8629–8631
13. Newton MA, Jyoti B, Dent AJ, Diaz-Moreno S, Fiddy SG, Evans J (2006) Chem Eur J 12:1975
14. Newton MA, Fiddy SG, Guilera G, Jyoti B, Evans J (2005) Chem Comm 1:118
15. Newton MA, Burnaby DG, Dent AJ, Diaz-Moreno S, Evans J, Fiddy SG, Neisius T, Pascarelli S, Turin S (2001) J Phys Chem A 105:5965
16. Newton MA, Burnaby DG, Dent AJ, Diaz-Moreno S, Evans J, Fiddy SG, Neisius T, Turin S (2002) J Phys Chem B 106:4214
17. Labiche J-C, Mathon O, Pascarelli S, Newton MA, Guilera Ferre G, Curfs C, Vaughan G, Homs A, Fernandez Carreiras D (2007) Rev Sci Instrum 78:091301
18. Newton MA (2007) J Synchrotron Rad 14:372–381
19. Binsted N (1988) PAXAS: programme for the analysis of X-ray adsorption spectra. University of Southampton, UK
20. Binsted N (1998) *EXCURV98*, CCLRC Daresbury laboratory computer programme
21. M Cavers, JM Davidson, IR Harkness, GS McDougall, LVC Rees (1999) In: Froment GF, Waugh KC (eds) Reaction kinetics and the development of catalytic processes, vol 122. Elsevier, Amsterdam, p 65
22. CN Satterfield, (1996) In: Heterogeneous catalysis in industrial practice, Krieger Publishing, USA
23. Arai H, Tominaga H (1976) J Catal 43:131–142
24. Liang J, Wang HP, Spicer LD (1985) J Phys Chem 89:5840
25. Srinivas G, Chuang SSC, Debnath S (1994) J Catal 148:748
26. Dictor R (1988) J Catal 109:89
27. Hyde EA, Rudham R, Rochester CH (1988) J Chem Soc Faraday Trans 80:531
28. Anderson JA, Millar GJ, Rochester CH (1990) J Chem Soc Faraday Trans 86:571
29. Yang AC, Garland CW (1957) J Phys Chem 61:1044
30. Yao C, Rothschild WG (1978) J Chem Phys 68:4774
31. Yates JT, Duncan TM, Worley SD, Vaughan RW (1979) J Chem Phys 70:1219
32. Antoniewicz PR, Cavanagh RR, Yates JT (1980) J Chem Phys 73: 3456
33. Basu P, Panayotov D, Yates JT (1988) J Am Chem Soc 110:2074
34. Cavanagh RR, Yates JT (1981) J Chem Phys 74:4150
35. Rice CA, Worley SD, Curtis CW, Guin JA, Tarrer AR (1981) J Chem Phys 74:6487
36. Van't Blik HFJ, Van Zon JBAD, Huizinga T, Vis JC, Koningsberger DC, Prins R (1983) J Phys Chem 87:2264
37. Suzuki A, Inada Y, Yamaguchi A, Chihara T, Yuasa M, Nomura M, Iwasawa Y (2003) Angew Chem Int Ed 42:4795
38. Bennett RA, McCavish ND, Basham M, Dhanak V, Newton MA (2007) Phys Rev Lett 98:056102
39. Cavers M, Davidson JM, Harkness IR, Rees LVC, McDougall GS (1999) J Catal 188:426
40. Kiss J, Solymosi F (1998) J Catal 179:277
41. Krisnamurthy R, Chuang SSC, Balakos MW (1995) J Catal 157: 512
42. Krisnamurthy R, Chuang SSC, Balakos MW (1996) J Phys Chem 99:16727
43. Solymosi F, Bansagi T (2001) J Catal 202:205
44. Schmatloch V, Jirka I, Kruse N (1991) J Chem Phys 100:8471
45. Sellmer C, Schmatloch V, Kruse N (1995) Catal Letts 35:165
46. Andersson S, Frank M, Sandell A (1998) J Chem Phys 108:2967
47. Mavrikakis M, Rempel J, Greeley J, Hansen LB, Norskov JK (2002) J Chem Phys 117:6737
48. Mavrikakis M, Baumer M, Freund HJ, Norskov JK (2002) Catal Letts 81:153
49. Als-Nielsen J, Grubel G, Clausen BS (1995) Nucl Instrum Methods B 97:522
50. Grunwaldt JD, Lutzenkirchen-Hecht D, Richwin M, Grundmann S, Clausen BS, Frahm R (2001) J Phys Chem B 105:5161
51. Duncan WD, Williams GP (1983) Appl Opt 22:2914
52. Williams GP, Hircshmugl CJ, Kneedler EM, Sullivan EA, Siddons DP, Chabal YJ, Hoffman F, Moeller KD (1989) Rev Sci Inst 60:2176

53. Williams GP, Dumas P (eds) (1997) Accelerator-based infrared sources and applications. Proceeding of the SPIE, 3153
54. Jamin N, Dumas P, Moncuit J, Fridman WH, Teillaud JL, Carr GL, Williams GP (1998) PNAS 95:4837
55. Guidi MC, Piccinini M, Marcelli A, Nucara A, Calvani P, Burattini E (2005) J Opt Soc Am A 22:2810
56. Marcelli A, Private communication
57. Stavitski E, Cox MHF, Swart I, De Groot FMD, Weckhuysen BM (2008) Angew Chem Intl Ed 47:1
58. Stötzel J, Lützenkirchen-Hecht D, Fonda E, De Oliveira N, Briois V, Frahm R (2008) Rev Sci Instr 79:083107
59. Frahm R, Stötzel J, Lützenkirchen-Hecht D (2009) Synchrotron Radiat News 22(2):6